Radiation Physics and Chemistry 167 (2020) 108347

Contents lists available at ScienceDirect

Radiation Physics and Chemistry

journal homepage: www.elsevier.com/locate/radphyschem

The use of personal protection equipment for the absorbed doses of eye lens and thyroid gland in CBCT exams using Monte Carlo

Maria Rosangela Soares[a,b,*], William S. Santos[a,c,d], Lucio P. Neves[c,d], Ana P. Perini[c,d], Wilson O.G. Batista[e], Ana F. Maia[f], Walmir Belinato[g], Linda V.E. Caldas[a]

[a] Instituto de Pesquisas Energéticas e Nucleares, Comissão Nacional de Energia Nuclear (IPENCNEN/SP), São Paulo, SP, Brazil
[b] Fundação Universidade Federal de Rondônia (UNIR), Porto Velho, RO, Brazil
[c] Instituto de Física, Universidade Federal de Uberlândia, Uberlândia, MG, Brazil
[d] Programa de Pós-Graduação em Engenharia Biomédica, Faculdade de Engenharia Elétrica, Universidade Federal de Uberlândia, MG, Brazil
[e] Departamento de Tecnologia em Saúde e Biologia - Instituto Federal da Bahia, Salvador, Bahia, Brasil
[f] Universidade Federal de Sergipe (UFS), Aracaju, SE, Brazil
[g] Departamento de Ensino, Instituto Federal de Educação, Ciência e Tecnologia da Bahia, Vitória da Conquista, BA, Brazil

ARTICLE INFO

Keywords:
CBCT
Monte Carlo simulation
Individual protection equipment
Anthropomorphic phantoms

ABSTRACT

The purpose of this study was to evaluate the absorbed dose in the thyroid and eye lens when the patient uses individual protection. For this purpose, Monte Carlo (MC) simulation was employed using five different field of view (FOV) sizes, available in the i-Cat classic CBCT equipment. To represent the patient, a male virtual anthropomorphic phantom was used. Three different models of lead eyewear and thyroid shield were evaluated, as well as the dose difference with and without the personal protection equipment. The difference in the absorbed dose in relation to the use of the lead eyewear presented a reduction of 19% for the 8 cm × 6 cm FOV (diameter × height), and 73% for the 14 cm × 22 cm FOV. In relation to the thyroid, only the shield that involved the whole neck contributed to the reduction of the absorbed dose by up to 72% for a 14 cm × 22 cm FOV. For the thyroid shields there was a maximum increase of 59% (14 cm × 6 cm FOV), consequently, increasing the effective dose for the protocol. The results showed that the lead eyewear contributed to the protection of the eye lens, but the efficiency of the thyroid shield depends on several factors, as FOV and shield model.

1. Introduction

Radiation protection is currently widely spread and essential in various radiological areas. In dental procedures, more rigid control, in relation to radiological protection, began effectively, after the introduction of cone beam computed tomography (CBCT). These exams present an average dose increase of approximately 100 μSv on the patient when compared with panoramic radiology procedures (Schulze et al., 2017). Furthermore, with the update of the tissue weighting factor (ω_T) values by the International Radiation Protection Commission (ICRP), including the salivary glands, oral mucosa, muscular lymph nodes, and extra thoracic airways in the list of radiosensitive tissues in publication ICRP 103 (2007), the effective dose, in dental radiological exams, increased between 32% and 422% (Tsapaki, 2017; Pauwels et al., 2014; Pauwels and Scarfe, 2018; Roberts et al., 2009). These facts, allied to the ALARA principle, support the radiological protection of the patient during a diagnostic procedure (Schulze et al., 2017).

The CBCT was introduced in dental radiology at the end of the XX century. Initially, only for dental procedures, it is now widely used for tomographic examinations of the neck, contributing to a better treatment of the patient (Tsapaki, 2017; Rottke et al., 2017). The CBCT technology, in addition of revolutionizing the practice of radiological dentistry, increased the dose on the patient. This is much more significant for children and adolescents, which corresponds to approximately 21% of the patients, and present a higher radiosensitivity when compared to adults (Tsapaki, 2017).

Due to the popularization of CBCT in radiological procedures (not only for dental procedures), several studies and recommendations were published (Pauwels et al., 2014; Roberts et al., 2009). Nevertheless, the national documents of several countries are not yet updated with protection procedures and guidance on the CBCT (Tsapaki, 2017). In this respect, there is the European Union with SEDENDEXCT project published by the European community publication, (EC, 2012), and the

* Corresponding author. Instituto de Pesquisas Energéticas e Nucleares, Comissão Nacional de Energia Nuclear (IPENCNEN/SP), São Paulo, SP, Brazil.
E-mail address: mrs@unir.br (M.R. Soares).

https://doi.org/10.1016/j.radphyschem.2019.108347
Received 13 December 2018; Received in revised form 24 May 2019; Accepted 29 May 2019
Available online 30 May 2019
0969-806X/

ICRP publication entitled “Radiological Protection in Cone Beam Computed Tomography” (ICRP - 129, 2015), which provides a guideline for safer use of CBCT.

In CBCT the field of view (FOV) size is one of the parameters that most affects the dose to which the patient is exposed. Its size directly influences the image quality due to X-ray scattering (EC, 2012; Pauwels et al., 2014). In most CBCT scans the thyroid and eye lens are within the primary radiation field, or are very close to it (ICRP - 129, 2015).

Among the various models available, in relation to the FOV, the equipment with personalized FOV and FOV pre-defined by the manufacturer stands out. There is no consensus, in the literature, on the use of protectors for the thyroid and eye lens of the patients (Rottke et al., 2017; ICRP - 129, 2015; Qu et al., 2012). In equipment with automatic exposure control (AEC), the use of personal protective equipment (PPE) that can be within the radiation FOV. This fact can greatly increase the radiation dose to the patient. Therefore, the use of these devices should be applied with caution, especially for a FOV very close to the eyes and thyroid (Goren et al., 2013). It should also be considered that the PPE cannot create image artefacts causing the repetition of the examination or impairing the diagnosis (EC, 2004). At the same time, the literature does not present consensus about the use of PPE during exposure in a dental CBCT (Schulze et al., 2017; Qu et al., 2012). In this sense, the purpose of this paper is to evaluate the absorbed dose in the thyroid and eye lens, for three different commercial models of thyroid protectors, and three models of lead eyewear during CBCT procedures.

2. Materials and methods

2.1. CBCT equipment

This study was conducted based on the CBCT i-Cat Classical equipment, manufactured by Imaging Sciences International, Hatfield, PA (ISI, 2010). It consists of an equipment with a 120 kV fixed tube voltage and 5 mA tube current (in the range 3–7 mA, depending on the installation). The minimum tube filtration corresponds to 10 mmAl. The equipment performs a 360° rotation for the acquisition of hundreds of 2D radiographs by exam. These devices work with the pulsed waveform, and the image voxel size is between 0.3 and 0.5 mm^3. The image acquisition consists of obtaining approximately 215 2D images. The current time product was 36.12 mAs and the distance between the source and the detector was 68.58 cm (ISI, 2010). The time for the 3D reconstruction is approximately 40 s. The i-Cat classical CBCT presents five factory predefined FOV sizes (diameter × height): 8 cm × 6 cm, 14 cm × 6 cm, 14 cm × 8 cm, 14 cm × 13 cm, and 14 cm × 22 cm.

Each FOV size is related to a different protocol. The 8 cm × 6 cm FOV was simulated to represent a localized exam for dental units in the anterior region of the mandible; the 14 cm × 6 cm FOV represented a mandible exam, including the submental region, irradiating great part of the thyroid; the 14 cm × 8 cm FOV represented a mouth exam; the 14 cm × 13 cm FOV irradiated part of the face, up to the eyes; and the 14 cm × 22 cm FOV irradiated the whole face. In all protocols the isocenter is located in the frontal portion of the mouth.

2.2. Anthropomorphic phantoms

Several phantoms may be used with Monte Carlo simulation. Among them, there are the mathematical phantoms (Snyder et al., 1978), voxel representations (López et al., 2019), image-based iterative reconstruction (Kawashima et al., 2019) and the MeSH type (Dong et al., 2019). The adult male virtual anthropomorphic phantom MeSH (MASH3) was used in this study. It was developed at the Department of Nuclear Energy of the Federal University of Pernambuco (DEN/UFPE) (Cassola et al., 2010). The characteristics follow the recommendations of the anatomical and physiological data for the reference man of the International Commission on Radiological Protection, ICRP 89 (ICRP-89, 2002). It has several organs, tissues and other structures with dosimetric importance. This phantom was built using the mesh surface concept, which allows the user to adjust the size of the organ of interest (Cassola et al., 2010). The main characteristics are: 73.0 kg (mass), 176.0 cm (height), 23.6 kg/m^2 (Body Mass Index), matrix size of 239 × 129 × 731 (columns × lines × slices) and voxel dimensions of 2.4 mm × 2.4 mm × 2.4 mm. One of its advantages is the geometry of the internal organs which are close to the real ones, leading to consistent results. The configuration of the MASH3 phantom arranged in the CBCT equipment is shown in Fig. 1.

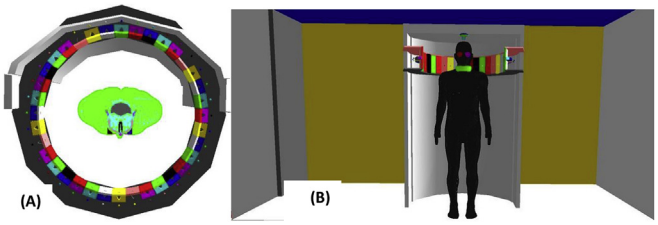

Fig. 1. Upper image of the position of the virtual anthropomorphic phantom in the CBCT equipment **(A)** and visualization of the phantom and CBCT device in the examination room **(B)**.

Since the MCNPX code is unable to calculate the energy absorbed on this type of surface, the phantoms of this class must necessarily undergo a process of voxelization of the entire structure. Mesh and hybrid phantoms (combining the stylized classes with voxel) constructed with the NURBS approach are part of a modern generation of phantoms. The organ volumes and anatomical details of these phantom classes can be adjusted. In addition, the flexibility of these phantoms enables the user to adjust the most appropriate posture and, thus, a more accurate representation of clinical exposure scenarios is achieved.

2.3. Personal protective equipment (PPE)

Three PPE models were used for this study (A, B and C). The arrangement of the protectors in the phantoms are shown in Fig. 2. The evaluation of the absorbed dose for each model, and the estimation of the effective dose, with the use of each model and set, were performed. The models were named A(E), B(E) and C(E) for the lead eyewears and A(T), B(T) and C(T) for the thyroid collars. Although many protectors indicated for use in dental radiology have a 0.25 mmPb thickness, in this study, only the 0.5 mmPb thickness was simulated. A description is presented in Table 1.

2.4. Monte Carlo simulations

In this study, the simulated X-ray tube, for the CBCT procedure, was simplified to a point source. To describe the rotational movement of the tube, 36 source positions were modelled, positioned 10° from each other. All sources were placed in the head and neck regions of the phantom, as delimited by the studied protocol. The photon energy spectrum, considering the bowtie filter and collimators, was generated using the SRS78 software (Cranley et al., 1997). This software generates spectral data for use in diagnostic radiology.

The results were obtained with the Monte Carlo code MCNPX 2.7.0 (Pelowitz, 2011), designed at the Los Alamos National Laboratory, USA. The MCNPX code was used to simulate the transport of photons, with the main interaction processes, including photoelectric absorption with the possibility of fluorescent emission and electron beam, coherent and incoherent scattering. In this study, only the transport of photons was considered. No variance reduction technique was used, and the remaining physical radiation transport parameters were maintained as the default in the MCNPX code. Aiming to reduce statistical uncertainties, 1×10^9 particle histories were used for each scenario. The MCNPX code has a set of cross section libraries with a wide range of energies, and it allows the user to model scenarios with three-

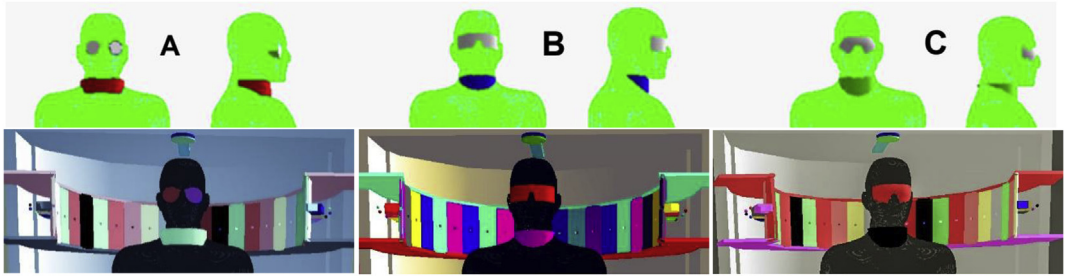

Fig. 2. Images of the types of thyroid protectors and lead eyewear (A, B and C) used in this study.

Table 1
Characteristics of the lead eyewear and the thyroid protecting collar used in this study.

Models	A	B	C
Lead Eyewear	Only crystalline shield	Frontal and lateral shield	Frontal shield without lateral protection
Collar thyroid	With side shield	Without side shield	With partial side shield

dimensional geometry. The library used in this work was the ENDF/B-VII.

In a previous study, a MC simulation scenario was developed using this CBCT device (Soares et al., 2019), in order to validate the geometry used, mainly the bowtie filter of which geometry is not easily found in the literature. More details regarding this validation may be found in the work of Soares et al. (2019). Three different PPE types, normally available at diagnostic radiology services, were used. Fig. 2 shows the arrangement of each protector.

2.5. Air kerma, absorbed and effective doses

For the measurement of the air kerma ($K_{air,measured}$), the Rapidose equipment (RADCAL® Corporation, Monrovia, CA, USA) was utilized. Air kerma measurements were experimentally taken, positioning the multidetector on the CBCT detector. The dose was then calculated for the isocenter of the equipment. The technical characteristics of the multisensor are: Rapidose Radical sensor, operating range 40 kV–150 kV, 2.5 mm Al and full filtration reading between 1 mm and 22 mm Al.

The absorbed dose was calculated from the conversion factor (CF), in particles/mAs. The validation of the CF was performed using the methodology of Gu et al. (2009) and Stratis et al. (2016), and demonstrated in a previous study (Soares et al., 2019). It is defined by Equation (1).

$$CF = \frac{K_{air,measured}}{K_{MC,simulated\ per\ particle}} \quad (1)$$

where $K_{air,\ measured}$ was determined at the isocenter of the CBCT device, with a current-time product of 36.12 mAs. In these conditions, the $K_{air,\ measured}$ was defined as mGy/36.12 mAs. The $K_{MC,simulated\ per\ particle}$ was obtained with the MC simulation at the same experimental conditions and units.

After obtaining the CF, the absorbed dose ($D_{absorbed}$) was determined for the tissues and organs, as suggested by the ICRP 103 (2007), for the virtual anthropomorphic phantoms using Equation (2):

$$D_{absorbed} = D_{simulated} \times CF \times N \quad (2)$$

where CF was obtained from Equation (1), $D_{simulated}$ is the value of tally F6 (in MeV/g/particle), and N represents the number of rotations of the equipment to acquire the image (in all scenarios, it was 1).

To determine the effective dose, it was necessary to define the equivalent dose to tissues and organs. Thus, the equivalent dose (H_T) was calculated as:

$$H_T = \omega_R . D_{absorbed} \quad (3)$$

In this Equation, $D_{absorbed}$ corresponds to the absorbed dose calculated in Equation (2) and ω_R corresponds to the radiation weighting factor ($\omega_R = 1$ for X-rays). The effective dose (E) was calculated using Equation (4), according to the methodology recommended by ICRP 110 (2009).

$$E = \sum_T \omega_T H_T \quad (4)$$

where the weighting factor ω_T was used for organs and tissues suggested by ICRP 103 (2007), and H_T is the equivalent dose of the organs and tissues of the male virtual anthropomorphic phantom.

3. Results and discussion

In an earlier experimental study, the thyroid accumulated between 11% and 18%, of the effective dose, in a range between 6.7 μSv and 19.9 μSv (corresponding to the range between 1.68E-01 mGy and 4.98E-01 mGy) for the equipment used in this study (Soares et al., 2015). This result was also obtained by other researchers, in previous studies (Qu et al., 2012; Pauwels et al., 2012; Morant et al., 2013). The eye lens was also in the primary beam, for some protocols. Regarding the absorbed dose in the eye lens, based on experimental studies, the values were between 6.1E-2 mGy and 8.0E-2 mGy (Pauwels et al., 2014). In this paper, the contribution of the thyroid for the effective dose was between 18% (14 × 8 FOV, with C(T)) and 48% (14 × 22 FOV, C(B)). The results presented in this study are within the experimental range, considering the differences in the positioning of the phantoms, and patients, uncertainties in the measurements, FOV and voxel sizes, and tube voltages.

Reducing the FOV size is an option available to reduce the radiation doses, without compromising the image quality. For this, most CBCT scanners have different FOV sizes. However, these sizes often cause the unnecessary irradiation of radiosensitive tissues (Qu et al., 2011). In the case of the CBCT i-Cat Classical apparatus, it has 5 different FOVs. This study examined the absorbed dose in the thyroid and eye lens for these FOV sizes, with the centre of the FOV in the frontal mouth region. The CF (Eq. (1)) for each studied FOV is presented in Table 2. As in a previous study (Soares et al., 2019), the current-time product used was 36.12 mAs, the tube voltage was 120 kV with a 3 mm Al filtration. The air kerma ($K_{air,measured}$) calculated for the isocenter of the CBCT

Table 2
CF used for the dose determination in the organs and tissues.

FOV [diameter × height] (cm × cm)	CF (particle/mAs)
8 × 6	2.34E+11
14 × 6	2.31E+11
14 × 8	1.73E+11
14 × 13	1.07E+11
14 × 22	6.39E+10

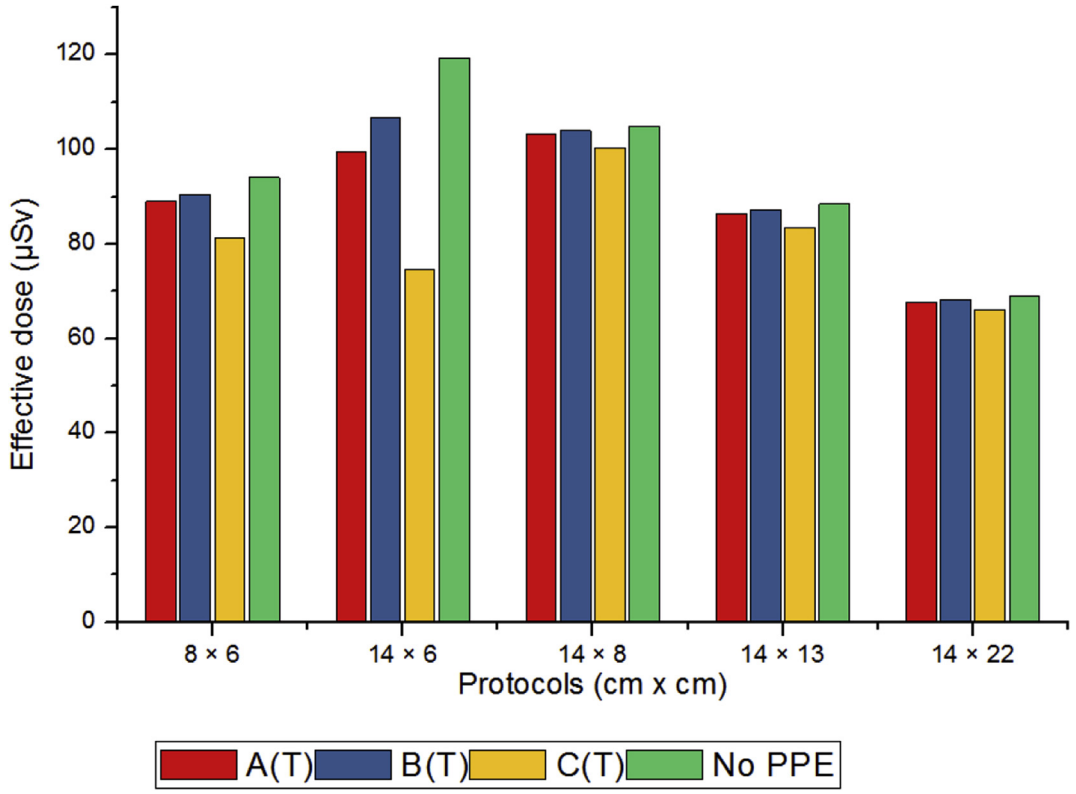

Fig. 3. Effective dose values with PPE (A(T), B(T) and C(T)) and without it.

equipment was 3.409 mGy.

The effective dose results with and without the PPE are shown in Fig. 3.

The effective dose is a risk indicator for patients exposed to ionizing radiation. However, according to the results of this study (Fig. 3), the use of the thyroid shield did not present a significant difference in the effective dose. Experimental studies by Rottke et al. (2017) and Schulze et al. (2017) also presented no statistical difference in the effective dose, when performing tests with and without a thyroid collar.

When analysing the shielding efficiency, the C(T) model presented better efficiency for effective dose reduction. In relation to the 14 cm × 6 cm FOV, the highest effective dose is likely to be related to the volume-of-interest (VOI) for the diagnosis (inferior arch) and to the isocenter of the FOV. Such results may be altered if the FOV is located in an upper region, for example, during an exam to visualize the axial sub-vertex, but not irradiating the submental region. In this case, the thyroid collar will not be irradiated, and the dose to the thyroid will be lower.

The absorbed doses in the thyroid and eye lens are presented in Table 3. There was no linearity between FOV size and effective dose, since different structures were irradiated, including the thyroid collar, in each FOV.

Considering the thyroid collars shielding properties, the A(T) and B (T) models were the least efficient in all protocols. For the 14 cm × 6 cm protocol, the use of the PPE increased the absorbed dose in the thyroid by almost 60%, with absorbed doses of 0.367 mGy for B (T) and 0.231 mGy (without PPE). For the 14 cm × 22 cm protocol, the use of the thyroid collar presented the highest efficiency. The absorbed dose for this protocol, in relation to the unshielded case, was reduced in 24% for the model B(T) and 73% for the C(T) model (Table 3).

Other studies draw attention to the use (or not) of the thyroid collar: 1. interference in the image, generating artefacts and forcing the exam repetition, increasing the dose in the patient (Tsapaki, 2017; EC, 2004); 2. the PPE is within the FOV, within the primary radiation field, increasing the dose in other organs due to the AEC (ICRP - 129, 2015; Goren et al., 2013); 3. the radiation that penetrates the posterior part of the neck, when the thyroid is inside the FOV, may generate backscattering radiation from the thyroid collar (which is located in the anterior part of the neck), leading to the inverse effect with the use of the collar (Pauwels and Scarfe, 2018). This effect occurred for the 14 cm × 6 cm FOV in the present work.

Rottke et al. (2017), in experimental studies, evaluated two CBCT devices. They did not find statistical differences, for the absorbed dose, in the thyroid with or without the collar. In the results of Hidalgo et al. (2015), the thyroid dose was reduced, however, in the condition of using two collars, covering the anterior and posterior part of the patient. Qu et al. (2012) demonstrated that the use of the thyroid collar during a CBCT exam, with 360° rotation, does not present a significant difference of absorbed dose in the thyroid. The ICRP 129 publication (ICRP - 129, 2015) entitled "CBCT: wide range of clinical applications and wide range of doses" recommends caution in the use of PPE for the eye lens, breast and thyroid. At the same time, this paper recommends evaluating the possibility of reducing the rotation-arc and the FOV size as efficient dose reduction actions. The MC simulation results of this paper agree with the results of other studies regarding thyroid shielding, and concludes that the dose reduction depends, in addition to the PPE model, on how the protector is used (Qu et al., 2011, 2012; Pauwels and Scarfe, 2018).

Using the lead eyewear, the absorbed dose for the eye lens was reduced by up to 73%, when compared to the same unshielded protocol. The results demonstrate that its use contributes to the reduction of the absorbed dose in the eyes lens. This result endorses the ICRP 129 (ICRP - 129, 2015) recommendation that emphasizes the need to optimize the protection for specific tissues, which includes the eye lens.

As discussed, the use of the thyroid collar and lead eyewear should be evaluated with criteria and responsibility since, in addition to interfering in the patient dose (if they are within the primary radiation field), they may even increase the dose, depending on the FOV. This study demonstrated that the absorbed dose in the thyroid is not advantageous in all FOV sizes, with or without the thyroid shield collar.

Table 3
Absorbed dose (mGy) in the eye lens and thyroid for the studied shield models. The absorbed dose reduction percentage was determined considering phantoms with and without the protectors. The uncertainties are presented in parenthesis (in %).

FOV (cm × cm)	*8 × 6*	*14 × 6*	*14 × 8*	*14 × 13*	*14 × 22*
A(T) (mGy)	*1.94E-01 (0.01)*	*3.57E-01 (0.01)*	*2.85E-01 (0.01)*	*3.84E-01 (0.01)*	*8.36E-01 (0.01)*
Difference from the unshielded thyroid	*12%*	*−55%*	*15%*	*23%*	*36%*
B(T) (mGy)	2.01E-01 (0.01)	3.67E-01 (0.01)	2.96E-01 (0.01)	4.11E-01 (0.01)	9.88E-01 (0.01)
Difference from the unshielded thyroid	9%	−59%	11%	18%	24%
C(T) (mGy)	1.65E-01 (0.01)	3.05E-01 (0.01)	2.29E-01 (0.01)	2.39E-01 (0.01)	3.57E-01 (0.01)
Difference from the unshielded thyroid	55%	−32%	31%	52%	72%
Unshielded thyroid (mGy)	**2.21E-01 (0.08)**	**2.31E-01 (0.08)**	**3.33E-01 (0.08)**	**5.01E-01 (0.08)**	**1.30E+00 (0.08)**
A(E) (mGy)	1.49E-02 (0.03)	1.86E-02 (0.03)	2.72E-02 (0.03)	4.80E-02 (0.03)	5.89E-02 (0.03)
Difference from the unshielded eye lens	25%	63%	32%	53%	58%
B(E) (mGy)	1.36E-02 (0.03)	1.65E-02 (0.03)	2.52E-02 (0.03)	3.54E-02 (0.03)	3.87E-02 (0.03)
Difference from the unshielded eye lens	32%	67%	37%	65%	73%
C(E) (mGy)	1.62E-02 (0.03)	1.95E-02 (0.03)	3.01E-02 (0.03)	6.17E-02 (0.03)	8.11E-02 (0.03)
Difference from the unshielded eye lens	19%	61%	25%	40%	42%
Unshielded eye lens (mGy)	**1.99E-02 (0.08)**	**5.03E-02 (0.08)**	**4.00E-02 (0.08)**	**1.02E-01 (0.08)**	**1.41E-01 (0.08)**

Considering that a significant part of all CBCT equipment available on the market has pre-defined FOV sizes, there must be a balance between the CBCT and another imaging modalities. Furthermore, it is indicated that the equipment allows personalized FOV sizes, allowing the delimitation of the radiosensitive organs.

4. Conclusions

This study showed that, for equipment with pre-defined FOV sizes, the thyroid collar reduces the dose in some protocols, but in the 14 cm × 6 cm protocol, used for evaluation of the lower dental arch, its use increased the absorbed dose to the thyroid. The use of lead eyewear contributed to the reduction of the absorbed dose in all protocols. Among the thyroid collars evaluated, the least indicated is the B(T) model, and the most recommended model is the C(T) model, as long as it is used is the appropriated protocols. The most efficient lead eyewear corresponds to the C(E) model. In relation to the effective dose, the use of the thyroid shield was irrelevant for the eye lens doses. This study demonstrated that the use of the protective collar did not lead to a dose reduction to the thyroid in all protocols; the authors of this study consider that the use of adequate shielding by the patient in CBCT procedures should be performed, whenever possible.

Acknowledgments:

The authors would like to thank Dr. Richard Kramer for kindly providing the virtual anthropomorphic phantoms; FAPEMIG (Grants Nos. APQ-03049-15 and APQ-02934-15); and CNPq (Grants Nos. 421603/2016-0, 420699/2016-3, 168947/2017-0, 150525/2016-8 and 30135/2016-8).

References

Cassola, V.F., Kramer, R., Brayner, C., Khoury, H.J., 2010. Posture-specific phantoms representing female and male adults in Monte Carlo-based simulations for radiological protection. Phys. Med. Biol. 55 (15), 4399–4430. https://doi.org/10.1088/0031-9155/55/15/014.

Cranley, K., Gilmore, B.J., Fogarty, G.W.A., Desponds, L., 1997. Catalogue of Diagnostic X-Ray Spectra and Other Data. Institute of Physics and Engineering in Medicine (IPEM) IPEM Report No 78.

Dong, L., Wijesinghe, P., Sampson, D.D., Kennedy, B.F., Munro, P.R.T., Oberai, A.A., 2019. Volumetric quantitative optical coherence elastography with an iterative inversion method. Biomed. Opt. Express 10 (2), 384–398. https://doi.org/10.1364/BOE.10.000384.

EC European Commission, 2004. Guidelines on Radiation Protection in Dental Radiology. Radiation Protection Report 136, Luxembourg.

E.C., European Commission, 2012. Radiation Protection No. 172: Evidence Based Guidelines on Cone Beam CT for Dental and Maxillofacial Radiology. Office for Official Publications of the European Communities, Luxembourg.

Goren, A., Prins, R., Dauer, L., Quinn, B., Al-Najjar, A., Faber, R.D., Patchell, G., Branets, I., Colosi, D.C., 2013. Effect of leaded glasses and thyroid shielding on cone beam CT radiation dose in an adult female phantom. Dentomaxillofacial Radiol. v42 (6), 20120260. https://doi.org/10.1259/dmfr.20120260.

Gu, J., Bednarz, B., Caracappa, P.F., Xu, X.G., 2009. The development, validation and application of a multidetector CT (MDCT) scanner model for assessing organ doses to the pregnant patient and the fetus using Monte Carlo simulations. Phys. Med. Biol. 54 (9), 2699–2717. https://doi.org/10.1088/0031-9155/54/9/007.

Hidalgo, A., Davies, J., Horner, K., Theodorakou, C., 2015. Effectiveness of thyroid gland shielding in dental CBCT using a paediatric anthropomorphic phantom. Dentomaxillofacial Radiol. 44 (3), 20140285. https://doi.org/10.1259/dmfr.20140285.

ICRP-89, 2002. Basic anatomical and physiological data for use in radiological protection reference values. Ann. ICRP 32 (3–4).

ICRP-103, 2007. The 2007 recommendations of the international commission on radiological protection. Ann. ICRP 37 (2–4).

ICRP-110, 2009. International commission on radiological protection. Publication adult reference computational phantoms. Ann. ICRP 39 (2).

ICRP-129, 2015. International commission on radiological protection. Radiological protection in cone beam computed tomography (CBCT). ICRP publication 129. Ann. ICRP 44 (1).

ISI Imaging Sciences International - Operator's Manual, 2010. Cone Beam Volumetric Tomography and Panoramic Dental Imaging System. Imaging Sciences International, Hatfield, PA Tech. Rep. Part number 990310 - Rev A.

Kawashima, H., Ichikawa, K., Matsubara, K., Nagata, H., Takata, T., Kobayashi, S., 2019. Quality evaluation of image-based iterative reconstruction for CT: comparison with hybrid iterative reconstruction. J. Appl. Clin. Med. Phys. https://doi.org/10.1002/acm2.12597.

López, M.A., Nogueira, P., Vrba, T., Tanner, R.J., Rühm, W., Tolmachev, S.Y., 2019. Measurements and Monte Carlo simulations of 241Am activities in three skull phantoms: eurados-ustur collaboration. Health Phys. https://doi.org/10.1097/HP.0000000000001080.

Morant, J.J., Salvadó, M., Hernández-Girón, I., Casanovas, R., Ortega, R., Calzado, A., 2013. Dosimetry of a cone beam CT device for oral and maxillofacial radiology using Monte Carlo techniques and ICRP adult reference computational phantoms. Dentomaxillofacial Radiol. 42 (3), 92555893. https://doi.org/10.1259/dmfr/92555893.

Pauwels, R., Zhang, G., Theodorakou, C., Walker, A., Bosmans, H., Jacobs, R., Bogaerts, R., Horner, K., SEDENTEXCT, Project Consortium, 2014. Effective radiation dose and eye lens dose in dental cone beam CT: effect of field of view and angle of rotation. Br. J. Radiol. 87, 20130654. https://doi.org/10.1259/bjr.20130654.

Pauwels, R., Scarfe, W.C., 2018. Radiation dose, risks, and protection in CBCT. In: Scarfe, W.C., Angelopoulos, C. (Eds.), Maxillofacial Cone Beam Computed Tomography. Springer, Cham, New York, NY, USA, pp. 227–246.

Pauwels, R., Theodorakou, C., Walker, A., Bosmans, H., Jacobs, R., Horner, K., Bogaerts, R., Sedentexct Project Consortium, 2012. Dose distribution for dental cone beam CT and its implication for defining a dose index. Dentomaxillofacial Radiol. 41 (7), 583–593. https://doi.org/10.1259/dmfr/20920453.

Pelowitz, D.B., 2011. MCNPX User's Manual, Version 2.7.0, Report LA-CP-11- 00438. Los Alamos National Laboratory, New Mexico, USA.

Qu, X.M., Li, G., Sanderink, G., Zhang, Z.Y., Ma, X.C., 2012. Dose reduction of cone beam CT scanning for the entire oral and maxillofacial regions with thyroid shields. Dentomaxillofacial Radiol. 41, 371–378. https://doi.org/10.1259/dmfr/30200901.

Qu, X.M., Li, G., Sanderink, G., Zhang, Z.Y., Ma, X.C., 2011. Thyroid shields for radiation dose reduction during cone beam computed tomography scanning for different oral and maxillofacial regions. Eur. J. Radiol. 81, 376–380. https://doi.org/10.1016/j.ejrad.2011.11.048.

Roberts, J.A., Drage, N.A., Davies, J., Thomas, D.W., 2009. Effective dose from cone beam CT examinations in dentistry. Br. J. Radiol. 82 (973), 35–40. https://doi.org/10.1259/bjr/31419627.

Rottke, D., Andersson, J., Ejima, K., Sawada, K., Schulze, D., 2017. Influence of lead apron shielding on absorbed doses from cone-beam computed tomography. Radiat. Protect. Dosim. 175 (1), 110–117. https://doi.org/10.1093/rpd/ncw275.

Schulze, R.K.W., Sazgar, M., Karle, H., De Las Heras Gala, H., 2017. Influence of a commercial lead apron on patient skin dose delivered during oral and maxillofacial examinations under cone beam computed tomography (CBCT). Health Phys. 13 (2), 129–134. https://doi.org/10.1097/HP.0000000000000676.

Snyder, W.S., Ford, M.R., Warner, G.G., 1978. Report ORNL-4979. Oak Ridge National Laboratory, Oak Ridge, TN, USA.

Soares, M.R., Batista, W.O., Antonio, P.L., Caldas, L.V.E., Maia, A.F., 2015. Study of effective dose of various protocols in equipment cone beam CT. Appl. Radiat. Isot. 100, 21–26. https://doi.org/10.1016/j.apradiso.2015.01.012.

Soares, M.R., Santos, W.S., Neves, L.P., Perini, A.P., Batista, W.O.G., Belinato, W., Maia, A.F., Caldas, L.V.E., 2019. Dose estimate for cone beam CT equipment protocols using Monte Carlo simulation in computational adult anthropomorphic phantoms. Radiat. Phys. Chem. 155, 252–259. https://doi.org/10.1016/j.radphyschem.2018.06.038.

Stratis, A., Zhang, G., Lopez-Rendon, X., Jacobs, R., Bogaerts, R., Bosmans, H., 2016. Customisation of a Monte Carlo dosimetry tool for dental cone-beam CT systems. Radiat. Protect. Dosim. 169 (1–4), 378–385. https://doi.org/10.1093/rpd/ncw024.

Tsapaki, V., 2017. Radiation protection in dental radiology – recent advances and future directions. Phys. Med. 44, 222–226. https://doi.org/10.1016/j.ejmp.2017.07.018.